Biomaterials 325 (2026) 123553

Contents lists available at ScienceDirect

Biomaterials

journal homepage: www.elsevier.com/locate/biomaterials

Tenascin-c functionalised self-assembling peptide hydrogels for critical-sized bone defect reconstruction

Alexandre Trubert-Paneli [a], Jonathan A. Williams [d], James F.C. Windmill [e], Leire Iturriaga [f], Eonan W. Pringle [a], Theodora Rogkoti [a], Siyuan Dong [h], Amaia Cipitria [f,g], Aline F. Miller [h], Cristina Gonzalez-Garcia [a], Alberto Saiani [i], Manuel Salmeron-Sanchez [a,b,c,*]

[a] Centre for the Cellular Microenvironment, Mazumdar-Shaw Advanced Research Centre, University of Glasgow, Glasgow, United Kingdom
[b] Institute for Bioengineering of Catalonia (IBEC), The Barcelona Institute for Science and Technology (BIST), Barcelona, 08028, Spain
[c] Institució Catalana de Recerca i Estudis Avançats (ICREA), Barcelona, Spain
[d] Centre for the Cellular Microenvironment, Department of Biomedical Engineering, University of Strathclyde, Glasgow, United Kingdom
[e] Department of Electronic and Electrical Engineering, University of Strathclyde, Glasgow, United Kingdom
[f] Group of Bioengineering in Regeneration and Cancer, Biogipuzkoa Health Research Institute, San Sebastián, Spain
[g] IKERBASQUE, Basque Foundation for Science, Bilbao, Spain
[h] Department of Chemical Engineering, School of Engineering, Faculty of Science and Engineering & Manchester Institute of Biotechnology, The University of Manchester, United Kingdom
[i] Division of Pharmacy and Optometry, School of Health Sciences, Faculty of Biology, Medicine and Health & Manchester Institute of Biotechnology, The University of Manchester, United Kingdom

A B S T R A C T

Critical-sized bone defects cannot heal spontaneously and receive poor clinical prognosis due to limitations in modern treatment strategies. Next-generation therapies are applying biomaterials incorporating BMP-2 to effectively promote and support bone regeneration, but adverse effects are linked to uncontrolled BMP-2 egress from the biomaterial. Implementing extracellular matrix proteins to biomaterials is a favourable approach to alleviate these drawbacks, and self-assembling peptide hydrogels are rapidly emerging as modulable and versatile biomaterials. Here, we describe the creation of a tenascin-c-functionalised peptide hydrogel designed to regenerate critical-sized bone defects. A recombinant fragment of tenascin-c spanning from the 3rd to 5th fibronectin-like domains is integrated into the fibre network. We demonstrate that this nascent construct effectively retains BMP-2 to differentiate mesenchymal stem cells into mature osteoblasts and achieves complete unionisation of murine critical-sized bone defects under low BMP-2 dose. All in all, we demonstrate tenascin-c as a suitable candidate to functionalise biomaterials intended for bone engineering applications and the promising potential of self-assembling peptide hydrogels in treating critical-sized bone defects.

1. Introduction

A critical-sized bone defect (CBD) is an injury beyond our natural regenerative capacity requiring surgical intervention to heal. The dilemma for a surgeon presented with a CBD is deciding whether to amputate or salvage the limb by autogenous bone grafting [1]. Unfortunately, limb salvage is restricted to 5 cm defects and imposes morbidity without guaranteeing a satisfactory outcome [2]. Allogenic grafts are also applied in such context, however they carry a risk of disease transmission and transplant rejection, and are limited in availability and customisability [1]. As an alternative, the field of tissue engineering focuses on applying biomaterials as synthetic grafts to promote and support bone regeneration. The INFUSE technology from Medtronic is an FDA-approved medical device for bone repair, described as a collagen sponge infused with bone morphogenetic protein 2 (BMP-2) [3]. BMP-2 is a potent growth factor commonly used to promote osteogenesis and has a well-documented mode of action. The limitation of INFUSE stems from its inability to confine BMP-2 within the collagen sponge, causing a spillage to the surrounding tissues and into the bloodstream, and leading to serious health risks such as ectopic bone formation, neurological dysfunction, and an increased risk of cancer [4]. As a pre-emptive measure, the BMP-2 dose in INFUSE is excessively high to provide an impact opportunity, which raises the treatment costs and the severity of the health risks. To tackle these

This article is part of a special issue entitled: European innovations published in Biomaterials.

* Corresponding author. Centre for the Cellular Microenvironment, Mazumdar-Shaw Advanced Research Centre, University of Glasgow, Glasgow, United Kingdom.
E-mail addresses: manuel.salmeron-sanchez@glasgow.ac.uk, msalmeron@ibecbarcelona.eu (M. Salmeron-Sanchez).

https://doi.org/10.1016/j.biomaterials.2025.123553
Received 3 March 2025; Received in revised form 9 July 2025; Accepted 10 July 2025
Available online 11 July 2025

challenges, there is a strong interest in endowing biomaterials with growth-factor-sequestrating capabilities to markedly reduce the BMP-2 dosage and alleviate the health risks and financial burden of treating CBDs with synthetic grafts.

The extracellular matrix (ECM) is the structural frame of native tissues and an essential medium for cell communication. Proteins that compose the ECM must be able to capture, store, and present cell-secreted molecules, termed cytokines, of which growth factors are a subset. ECM proteins such as fibronectin, laminin, or tenascin-c harbour a heparin-binding domain (HBD) in their composition; the extensive work of the Hubbell group showed that growth factors could promiscuously bind to the HBD of these proteins [5–7]. Moreover, it has been demonstrated that the proximity of the HBD to a cell adhesion motif can trigger the co-localised activation of growth factor and integrin receptors and instigate a synergistic effect, resulting in the prolongation of the growth factor signal and an amplification of the phenotypical response [8,9]. Fibronectin is well-established and has been extensively applied to biomaterials for its growth factor sequestration properties and eligibility to instigate the synergistic effect [9–11]. A lesser applied ECM protein, tenascin-c, shares a close homology to fibronectin [12]. The tenascin-c monomer consists of a linear chain of domains, categorised into types, including the 'fibronectin type III-like' domain type (TNCIII) [13]. The 3rd and 5th TNCIII domains respectively contain an RGD integrin-binding motif and an HBD [13,14]. Accordingly, it is hypothesised that the proximity of these domains can instigate the synergistic effect analogously to fibronectin; however, this has yet to be investigated. Thus, a fragment of tenascin-c spanning the 3rd to 5th TNCIII domain region may be a suitable candidate for bone engineering applications.

Hydrogels are polymeric biomaterials widely used in tissue engineering for their structural recapitulation of the fibrous ECM. Polymers composing hydrogels rarely harbour the desired functionalities; thus, it is common practice to integrate or tether bioactive molecules to the polymer network, a practice called hydrogel functionalisation. An otherwise non-functionalised molecule is anticipated to promptly leak out of the hydrogel before contributing an effect, as exemplified by the BMP-2 egress from INFUSE. Self-assembling peptide hydrogels (SAPH) arise in an aqueous environment from the spontaneous assembly of customised peptide building blocks to form a supramolecular fibre network [15]. The SAPH system emerged in the 1990s as a novel hydrogel system that synergises biocompatibility with reproducibility and fine tunability over physico-chemical properties [16]. SAPHs can be conveniently functionalised through a concept we term 'self--functionalisation'; it follows the rationale that a bioactive molecule of interest can be conjugated with the peptide building block to allow its incorporation in the fibre architecture [17]. Self-functionalisation is a low-cost, straightforward, and reproducible method widely applied across different types of self-assembling hydrogels [17–20].

In the present study, we report the conceptualisation, production, and evaluation of a SAPH functionalised with a tenascin-c fragment spanning from the 3rd to the 5th TNCIII domain. The aim of the functionalised SAPH is to effectively confine BMP-2 within the hydrogel and optimise its presentation at the cell/material interface via synergistic integrin/growth factor signalling. The base SAPH technology was appropriated from the $(FEFK)_2$ system, commercially available as Delta1 from Cell Guidance Systems [21]. The purpose of the functionalised SAPH is two-faceted; the first is to efficiently differentiate bone marrow-derived mesenchymal stem cells (MSCs) into osteoblasts *in vitro*, and the second is to promote the reconstruction of a murine critical-sized bone defect *in vivo*. In parallel, we assess the importance of fragment tethering by comparing the self-functionalised (tethered) and physically mixed (untethered) versions of the functionalised hydrogel and their implications for the *in vitro* and *in vivo* experiments proposed. The layout of this article follows the work pipeline from the production of the fragments and their characterisation in 2D to the assessment of self-functionalisation and hydrogel functionality in 3D. Subsequently, the functionalised gels were applied in an *in vitro* context to investigate the osteogenic differentiation of MSCs under BMP-2 treatment. Finally, the functionalised hydrogels were implemented in a mouse critical-sized defect model to investigate their ability for bone reconstruction *in vivo*. All in all, we advocate for the use of tenascin-c to efficiently sequester BMP-2 and to promote the synergistic effect. We also reveal the ability of both the bare and functionalised SAPH system to repair CBDs.

2. Results

2.1. The recombinant tenascin-c fragments conserve their functionality at the respective domains

The Delta1 SAPH system emerges from the assembly of peptides of amino acid sequence $(FEFK)_2$; the sequence has been designed to drive β-sheet-rich fibre formation via hydrogen bonding [21,22]. Hydrogel formation and fibre crosslinking is controlled through hydrophobic/hydrophilic and electrostatic fibre-fibre interactions [21,22]. The strong propensity of the peptides to assemble is exploited to functionalise a recombinant protein of interest to the fibre architecture (Fig. 1A), an approach previously reported for this SAPH system [17,23]. A library of tenascin-c fragments composed of F3, F5, F35, and T35 was established (Fig. 1B). The nucleotide sequence of tenascin-c was trimmed from the 3rd to the 5th TNCIII domains and accordingly endowed the peptide sequence at the C-terminal. The denotation 'F' in the fragment nomenclature notes the addition of the peptide building block and a capacity for self-functionalisation. The nucleotide sequence of the respective fragments was inserted in a pGEX-6P-1 vector harbouring a GST fusion tag for purification. The plasmids were transformed in Rosetta 2 pLysS/BL21-DE3 *E. Coli*. The 3rd, 4th, and 5th TNCIII domains are fortuitously sparse in post-translational modifications and could be recombinantly expressed at high yields and purity (Fig. 1C). The GST fusion tag was kept after fragment elution, as cleavage of the tag has been shown to diminish the functionality of the HBD [7].

The functionality of the HBD was assessed via sandwich ELISA assays. The first assessment evaluated the ability of the fragments to bind heparin via a GST ELISA using heparin and fragment as receptor and ligand, respectively (Fig. 1D). The assay confirmed the F5 and F35 fragments to have high binding for heparin, whereas the HBD-deprived F3 does not. However, T35, although endowed with an HBD, did not bind heparin. The heparin-binding site on the tenascin-c HBD has been identified as the sequence 1057-KGRHKSKPARVK-1068, located six amino acid positions away from the C-terminal of the 5th domain [14]. In the design of the T35 fragment, the sequence is abruptly terminated at the 1074th amino acid position and is anticipated to disturb the natural conformation of the fragment at the C-terminal edge and misfold the heparin-binding site; hence, incapacitating its ability to bind heparin. The fragments were subsequently assessed for their ability to bind BMP-2 (Fig. 1D). The BMP-2 ELISA applied the fragment as a receptor and BMP-2 as a ligand. Surprisingly, all fragments showed binding to BMP-2 despite F3 not having an HBD, suggesting that BMP-2 binding is not specific to the HBD and can also manifest at the 3rd domain; however, BMP-2 binding to F5, F35, and T35 was significantly higher than to F3. The experiment was reproduced with FGF-2 to determine whether growth factors generically bind to both the 3rd and 5th domains (Fig. 1D). FGF-2 did not bind to F3 but showed strong binding to F5, F35, and T35, suggesting that in the case of FGF-2, binding is specific to the HBD. Moreover, it shows that a non-functional heparin binding site, as observed with T35, does not prohibit growth factor binding.

The conservation of the adhesive properties at the 3rd domain was assessed by overnight incubation of the fragments in a tissue culture well plate. MSCs were seeded on the functionalised substrates and cultured for 2 h without FBS (Fig. 1E). Fragments harbouring the 3rd TNCIII domain demonstrate conspicuous cell spreading, whereas the F5 condition shows limited cell adhesion; quantification from the phalloidin signal indeed reveals a significantly higher cell spreading for the F3 and

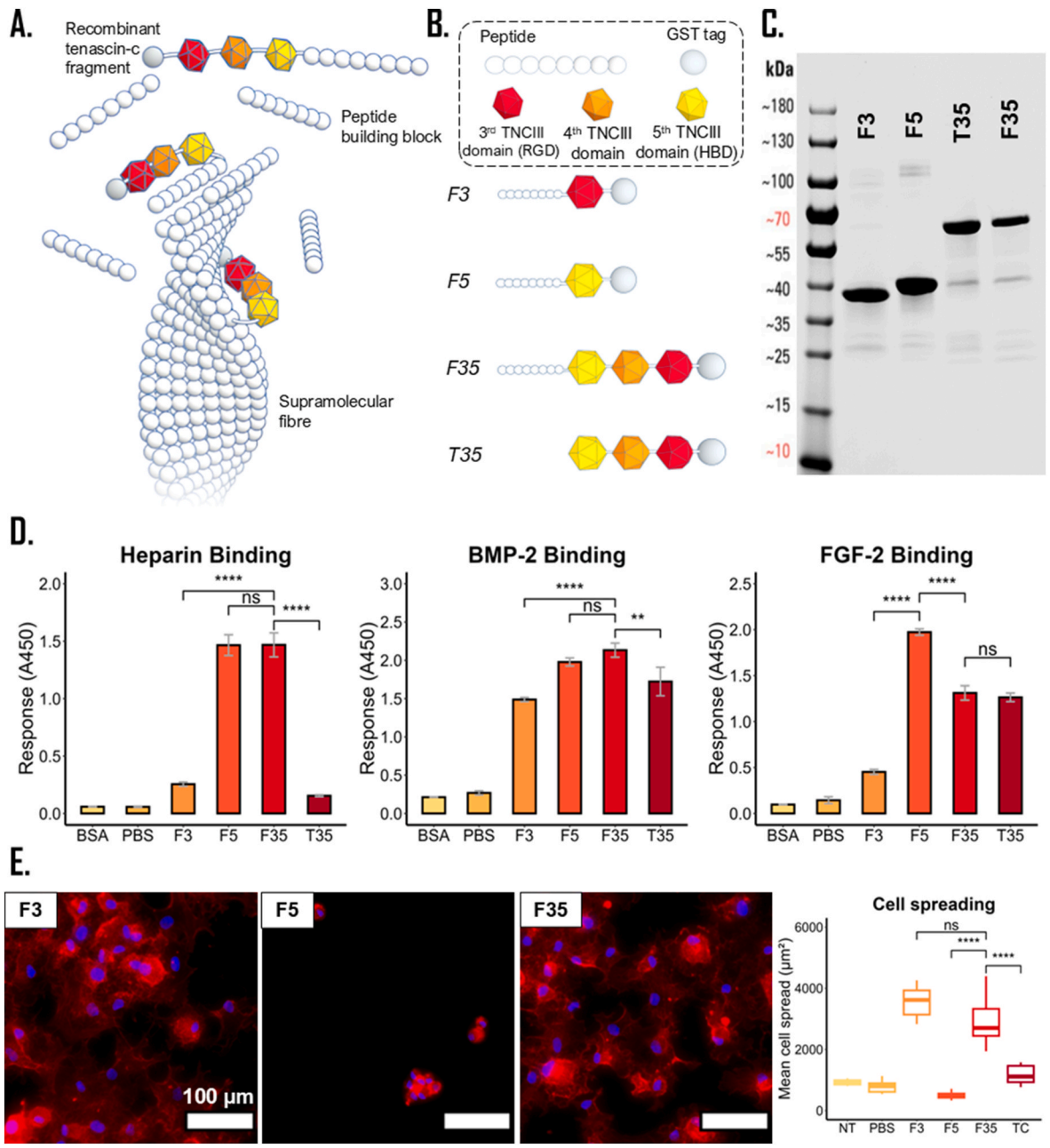

Fig. 1. The recombinant tenascin-c fragment library and functionality characterisation at the respective TNCIII domains. **A.** Illustration of the self-functionalisation concept. A recombinant fragment is produced with the peptide building block $(FEFK)_2$ at its C-terminal; the recombinant fragment is complemented to the peptide solution and integrates into the architecture of the self-assembled fibre. **B.** Illustration of the tenascin-c fragment library; individual components of the fragments are described in the dashed box. **C.** SDS-PAGE of the tenascin-c fragment library after purification. **D.** Solid-phase binding assessment of the fragment library for heparin, BMP-2, and FGF-2. **E.** Assessment of cell adhesion to fragment-functionalised substrates. Phalloidin is shown in red and DAPI in blue. Images were acquired with an LSM980 confocal microscope and analysed with ImageJ. Scale bar: 100 µm. 'NT' and 'TC' stand for 'non-treated' and 'tissue culture-treated' respectively. Error bars show the standard deviation. Statistical significance: $^{**}p < 0.01$, and $^{****}p < 0.0001$. (For interpretation of the references to colour in this figure legend, the reader is referred to the Web version of this article.)

F35 conditions, confirming the availability of the RGD motif. Thus, the characterisation assays attest for the sustainable production of the fragments and the preservation of their functionality at the respective domains. From here on, the focus was narrowed to the F35 and T35 fragments to investigate the synergistic effect and the importance of protein tethering in osteogenic applications.

2.2. The tenascin-c fragments functionalise the fibres by self-functionalisation

The Delta1 hydrogel was received from Cell Guidance Systems as a ready-to-use viscous peptide solution; the gel was functionalised by adding in the fragment solution at the desired concentration. The F35 hydrogel was prepared at a final fragment concentration of 1 mg/mL; the other hydrogel groups were prepared as to match the molarity of the F35 hydrogel. The hydrogels were stable for 21 days in cell culture conditions (Supporting Information Figure S1). A Fourier transform

infrared spectroscopy (FTIR) analysis was conducted to compare the structure of the respective fibres and confirm that the introduction of the fragments did not affect the ability of the peptides to self-assemble into β-sheet rich fibres (Fig. 2B). The samples were measured in the absorbance range of 1400–1800 cm^{-1}, with particular focus on the peaks at 1620 and 1685 cm^{-1}, denoting the adoption of β-sheet structures [24]. The spectra under all conditions are comparable, confirming that for all hydrogel groups, the ability of the peptides to self-assemble into β-sheet rich fibres is conserved. The fibres of the Delta1, F35, and T35 hydrogels were imaged with transmission electron microscopy (TEM) to witness self-functionalisation (Fig. 2A). Diluted hydrogel samples were fixed on a carbon-coated copper grid and negatively stained. Imaging of the bare Delta1 hydrogel shows well-defined smooth fibres with an approximate width of 4 nm, consistent with the literature [21,25]. In contrast, the fibres in the F35 hydrogel show periodical units branching off the fibre thought to be self-functionalised fragments (denoted by red arrows in figure). Observations of the T35 fibres did not reveal any units branching from the fibres and instead showed smooth fibres analogously to Delta1.

The functionalisation of F35 was next assessed through a fragment release experiment, where the release of fragments from the F35 and T35 hydrogels was measured over 7 days of incubation in cell culture conditions. The functionalised hydrogels were prepared at 1 mg/mL, seeded with MSCs at 1 million cells/mL, submerged in PBS, and maintained in cell culture conditions; the PBS was collected and replenished every 24 h for 7 days. The evolution of fragment release throughout the time points was revealed through a GST ELISA, using the concentration-known fragment stock to establish the standard curve (Fig. 2C). The experiment was initially conducted in the absence of MSCs and resulted in no significant difference between hydrogel groups (Supporting Information Figure S2). The iteration of the experiment with MSCs reveals that the F35 and T35 hydrogels respectively released ≈10 and ≈15 % of their fragment content after 7 days. The surprising result was witnessing the untethered T35 fragment remaining confined in the hydrogel system long-term with limited leakage, which is in contrast to previous reports where an enzyme of a similar molecular mass has been shown to promptly leak from an analogous SAPH system [17]. The high retention is thought to stem from the small mesh size of the fibre network (between 10 and 20 nm) [26], sterically entrapping bulky proteins such as T35.

A rheological evaluation of the hydrogel groups was conducted to measure their respective storage modulus and loss tangent (tanδ) (Fig. 2D). The assessment shows a significant distinction in the stiffness of the hydrogels, with Delta1, F35, and T35 demonstrating a respective storage modulus of ≈500, ≈2400, and ≈1700 Pa. The increase in hydrogel stiffness from the physical addition of T35 suggests an interaction between fragment and fibre, however, where the fragment enhanced hydrogel rigidity, it did not have a significant impact on the viscous character. In contrast, the addition of F35 further raised the hydrogel stiffness and significantly lowered the tanδ; considering the fragments have marginal differences in their molecular mass, these observations suggests that the nature of the F35/fibre interaction is different to that of T35 and corroborates the occurrence of self-functionalisation.

2.3. The functionalised hydrogels display enhanced bioactivity

Following the characterisation of the F35 fragment and the evaluation of self-functionalisation, we assessed the F35 hydrogel for its ability to instigate cell spreading and confine growth factors. The ability of the Delta1, F35, and T35 hydrogels to confine BMP-2 was determined via a BMP-2 release assay (Fig. 2E); the hydrogels were supplemented with BMP-2 at 5 μg/mL, and the release of growth factors was quantified every 24 h throughout 120 h. The plain Delta1 hydrogel released ≈20 % of its BMP-2 content after 24h of incubation; in contrast, the F35 and T35 hydrogel groups released ≈3.5 and ≈ 7 % of their BMP-2 content respectively, demonstrating the ability of the fragments to capture BMP-2. After 120 h of incubation, the supplemented F35 and T35 hydrogels retained a remarkable 92 and 85 % of their BMP-2 contents respectively, whereas Delta1 retained 60 %. The viability of encapsulated MSCs was evaluated over 7 days for the Delta1, F35, and T35 hydrogel groups (Fig. 2F). The viability assay distinguished between the core and mantle of the hydrogel to assess the ability of each microenvironment to sustain cell life. The mantle was defined as the 300 μm zone immediately under the gel/media interface, the hydrogel being dome-shaped with a height of ≈3 mm and a diameter of ≈4.5 mm. A dense hydrogel mesh presents an obstacle to nutrient and oxygen permeability into deeper zones of the construct; the core will be more nutrient-deprived and hypoxic than the near-surface mantle zone. Therefore, a comprehensive assessment of viability requires a distinction in hydrogel loci. The results show that viability at the mantle is between 80 and 90 % for all hydrogel groups over 7 days, indicating that all hydrogels can accommodate cell populations regardless of functionalisation and that the base hydrogel technology is biocompatible. A distinction becomes apparent at the core of the hydrogel, where Delta1-encapsulated cells gradually lose viability over time, with viabilities of 58, 50, and 21 % on Day 1, 3, and 7, respectively. The absence of integrin binding domains in the Delta1 hydrogel renders the cells inactive, as they are wrapped in fibres, unable to effectively sense their surroundings or migrate; the MSCs are thus speculated to stay entrapped and gradually succumb over the 7 days. On the other hand, the functionalised hydrogel groups displayed a viability at the inner core between 80 and 90 % analogously to the viability at the mantle, indicating that the presence of integrin binding sites on the fibres increases cell survival; this is in good agreement with a study by Clark and colleagues (2020) where they compare MSC viability between adhesive and non-adhesive hydrogels [27].

The adhesive properties were quantified by encapsulating MSCs in the hydrogel groups and culturing them in non-inducing conditions for 3 days (Fig. 2G). Cell adhesion within the hydrogels was quantified by a circularity score from 1 to 0, where 1 represents a perfect circle and lower values approaching 0 denote an increasing elongation, irregularity, and asymmetry. Encapsulated cells in the Delta1 group assumed a round morphology with a mean circularity of 0.83, consistent with the lack of integrin binding sites. On the other hand, the elongated cells in the F35 hydrogel exhibited a mean circularity of 0.47, reflecting a significant cell adhesion and spreading in the hydrogel matrix. Expectedly, a minor degree of cell elongation is observed in the T35 hydrogels with a mean circularity of 0.69; since the T35 fragment is not functionalised to the fibres, it does not offer the mechanical resistance required for the cells to pull and achieve a stretched and elongated configuration. These observations lead to the interpretation that F35 and T35 can efficiently present the RGD motif to promote adhesion, and the immobilisation of F35 to the fibre proffers the mechanical resistance required to enable cell stretching.

2.4. The functionalised hydrogels efficiently induce osteogenesis in vitro

The F35 hydrogel demonstrated a strong capacity to confine BMP-2 and enable MSC adhesion; we tested these features in an osteogenesis experiment where MSCs were encapsulated in the Delta1, F3, F35, and T35 hydrogels, stimulated with BMP-2 at 5 μg/mL, and cultured *in vitro* for 21 days. The BMP-2 was administrated on Day 0, and the MSCs did not benefit from subsequent exogenous growth factor administrations. The encapsulated cells at each time point were analysed for their phenotype and genotype with staining and qPCR, respectively. Moreover, an Alizarin red staining was performed on Day 21 to visualise calcium deposition in hydrogel sections. Cell morphology on Day 21 reveals distinct phenotypes across the hydrogel groups (Fig. 3A). The F35 hydrogel displays highly stretched cells with prevalent cell-to-cell interaction reminiscent of the osteoblastic phenotype [28]. In contrast, the cells in Delta1 are isolated from each other and adopt a round configuration. The cells in the F3 and T35 hydrogels have a morphology

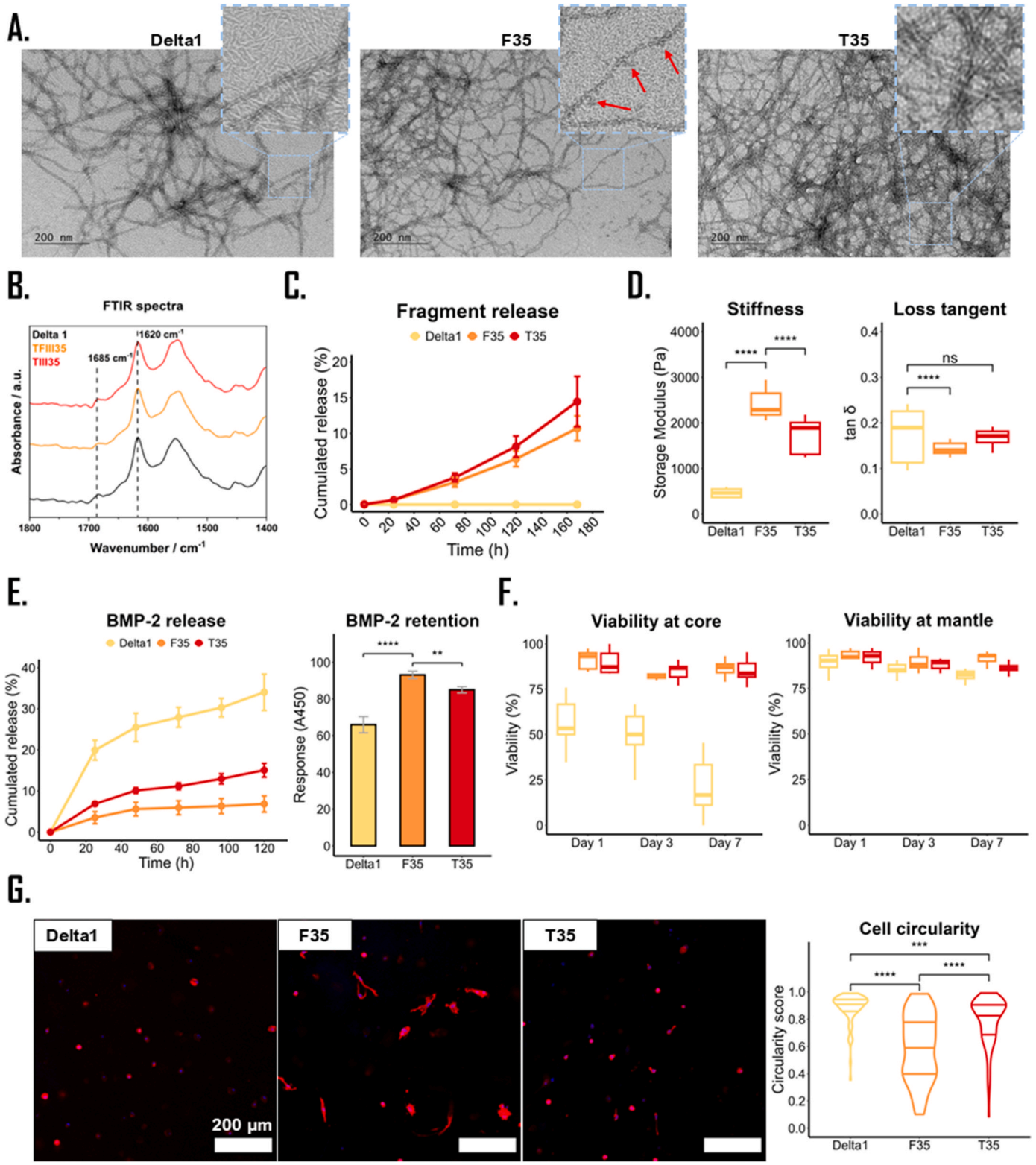

Fig. 2. Hydrogel self-functionalisation, functionality, and biocompatibility. **A.** TEM imaging of fibres from the Delta1, F35, and T35 hydrogel groups. The red arrows in F35 show noticeable branchings off the fibres. Scale bar: 200 nm. **B.** FTIR spectra of the Delta1, F35, and T35 hydrogels between 1400 and 1800 cm^{-1}. **C.** Fragment release over 7 days from the functionalised hydrogels encapsulated with MSCs. **D.** Stiffness and loss tangent for the Delta1, F35, and T35 hydrogels. **E.** BMP-2 release from the Delta1, F35, and T35 hydrogels over 120 h; initial BMP-2 concentration was 5 µg/mL in 20 µL gels (i.e. 100 ng of BMP-2 per replicate). **F.** MSC viability within the Delta1, F35, T35 hydrogels over 7 days. **G.** Assessment of cell adhesion in the Delta1, F35, and T35 hydrogels after 3 days of culture. Phalloidin is shown in red and DAPI in blue. Images were acquired with an LSM980 confocal microscope and analysed with ImageJ. Scale bar: 200 µm. Error bars show the standard deviation. Statistical significance: $^{**}p < 0.01$, $^{***}p < 0.001$, and $^{****}p < 0.0001$. (For interpretation of the references to colour in this figure legend, the reader is referred to the Web version of this article.)

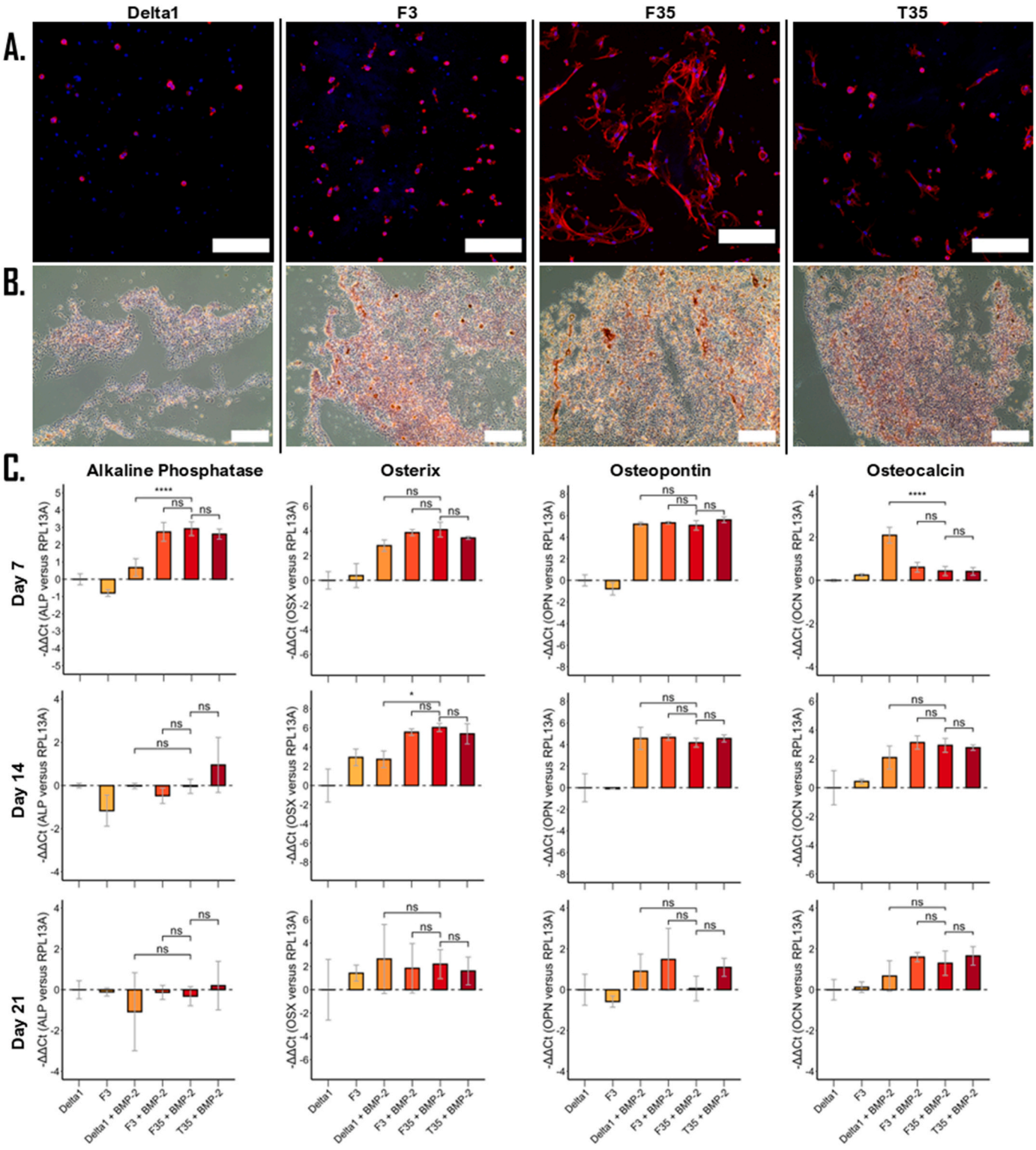

Fig. 3. Osteogenic differentiation of MSCs *in vitro*. **A.** Staining of MSCs encapsulated in the hydrogel groups with BMP-2 for 21 days. Phalloidin is shown in red and DAPI in blue. Images show a ≈183 μm tall z-stack, stacked into one frame. Images were acquired with an LSM980 confocal microscope and analysed with ImageJ. Scale bar: 200 μm. **B.** Staining of calcium deposits in the hydrogel groups with BMP-2 for 21 days. Hydrogels were cryosectioned (20 μm) and stained with Alizarin red (40 mM, pH 4.2). Images were acquired with an EVOS XL Core. Scale bar: 200 μm. **C.** qPCR analysis of osteogenic markers from MSCs encapsulated in the hydrogel groups with BMP-2 for 7, 14, and 21 days. Tested genes were alkaline phosphatase, osterix, osteopontin, and osteocalcin. The Delta1 condition serving as negative control is shown on the left and displays the basal expression level. Error bars show the standard deviation. Statistical significance: *$p < 0.05$ and ****$p < 0.0001$. (For interpretation of the references to colour in this figure legend, the reader is referred to the Web version of this article.)

between these two extremes with noticeable cell spreading, however, neither reached the phenotype of F35. Cells encapsulated in Delta1 consistently exhibited round morphologies throughout the 21 days of culture (Supporting Information Figure S3). It is important to note that MSCs have been reported to osteogenically differentiate whilst retaining a round configuration [29]; however, it is difficult to perceive these cells sustaining osteoblastic function.

The differentiation of MSCs to mature osteoblasts entails the sequential upregulation of osteogenic genes that researchers commonly use as markers to monitor its progression [30]. At each time point, mRNA was extracted from the samples and measured by qPCR for the osteogenic markers bone alkaline phosphatase (ALP), osterix (OSX), osteopontin (OPN), and osteocalcin (OCN) (Fig. 3C). ALP is an early marker expressed in the first days of *in vitro* induction, OSX and OPN are intermediate markers contributing to ECM deposition, and OCN is a late marker of mineral deposition [31–35]. Results on Day 7 reveal a significant upregulation of ALP, OSX, and OPN for the functionalised hydrogels with BMP-2 compared to the unstimulated Delta1 control, suggesting a successful induction to the osteogenic lineage [32]. The upregulation of OSX and OPN carries over to Day 14, along with an upregulation of OCN, indicating that osteoblasts are reaching maturation [35]. The upregulation of OSX and OCN is sustained over to Day 21. The gene expression profile of osteogenic differentiation in this experiment aligns with previous reports in the literature [30,36]; however, there are marginal statistical differences between the bare Delta1 + BMP-2 versus the functionalised hydrogel + BMP-2. These observations reveal that MSCs encapsulated in Delta1 and treated with BMP-2 have an osteoblastic genotype and that adhesion and cell-to-cell interactions are not prerequisites for osteogenic differentiation. As observed in the BMP-2 release assay, Delta1 has an intrinsic ability to sequester the growth factor over 5 days, long enough for BMP-2 to stimulate the MSCs; it is therefore suggested that the high baseline of BMP-2 retention in these peptide hydrogels will initiate osteogenic differentiation regardless of the functionalisation proffered. Nevertheless, gene expression does not systematically translate to proteome and functionality as many osteogenic activities are contingent on a spread cell surface area and prevalent cell-to-cell interactions [37–39]. This is evidenced by the Alizarin red staining of the hydrogels (Fig. 3B), which reveals prevalent calcium deposits in the functionalised hydrogel groups, but only sparse deposition in the Delta1 + BMP-2 condition. Among the functionalised hydrogel groups, calcium deposits are most prominent in F35, where they appear in characteristic ridges or trails; this pattern is in congruity with the phenotype observed in the F35 hydrogel. Thus, the combination of the genotype, phenotype, and molecular output analyses indicates that cells in the functionalised hydrogels are functional osteoblast. Notably, the data demonstrates that inducing the synergistic effect through co-localised integrin and growth factor signalling produces a relevant and performant osteoblastic model as seen in F35.

2.5. The SAPH system promotes bone regeneration in vivo

The F35 fragment improved the osteogenic potential of the Delta1 hydrogel platform *in vitro*. Next, we investigated whether these results could be replicated *in vivo* using the well-established mouse radial CBD model [11,40–43]. Specifically, a reproducible 2.5 mm-long bone defect was created at the centre of the radius. The defect was stabilised by fitting a non-degradable 4 mm-long porous polyimide tube to the two bone ends of the defect, stabilising them. The hydrogel systems previously described were loaded into the implant tube before fitting. Five experimental conditions were tested, these include: Delta1, F35, Delta1 + BMP-2 (10 μg/mL), F35 + BMP-2 (10 μg/mL), T35 + BMP-2 (10 μg/mL) (all with low dose BMP-2), and a collagen gel + BMP-2 (75 μg/mL - high dose BMP-2) group serving as the positive control. Eight weeks after implantation, the mice were sacrificed, and the forearm bones were scanned by micro-computed tomography (μCT) to reveal the extent of bone regeneration, followed by histological evaluation with Goldner's trichrome staining (Fig. 4A). μCT scans were analysed to compute the gap length (Fig. 4B), the bone volume fraction in the central 2 mm of the defect (Fig. 4C), the number of animals displaying a unified bone marrow cavity (Fig. 4D), and the tissue mineral density (Supporting Information S4). The μCT scans of all defects are shown in the Supporting Information Figure S5. An Alcian Blue with Picrosirius Red histological staining under brightfield and polarised light is shown in Fig. 5.

Statistical analyses using ANOVA did not reveal significant differences between groups, mainly due to increased variance caused by outliers. However, the group medians suggest consistent patterns in regenerative performance. No sex-related differences in regeneration were observed. The μCT scans reveal that the Delta1 and F35 conditions without BMP-2 regenerated a substantial portion of the defect without unionisation; on average, Delta1 regenerated 86.8 % ± 10.5 of the bone defect and 84.3 % ± 14.2 for F35 (calculated from the remaining gap length). This extent of regeneration is analogous to the results seen in the literature using collagen sponges or PEG hydrogels with 5 μg/mL BMP-2 [11,40], and highlights the innate ability of the SAPH platform to drive bone reconstruction. The Delta1 and F35 conditions loaded with low dose BMP-2 consistently achieved healing as defined by a connected bone marrow cavity throughout the regenerated diaphysis. Impressively, the extent of bone reconstruction reported in these groups with low-dose BMP-2 is comparable to the positive control with high dose BMP-2. Histology confirmed these findings, showing mineralised tissue within the critical-sized defects; a connected bone marrow cavity running through the fused radial diaphysis confirmed the cases of complete bridging. Polarised light imaging shown in Fig. 5 reveals thick, mature collagen type I fibres in red, and thinner, immature fibres—characteristic of collagen type III—in green [44]. The native cortical bone adjacent to the defect displays densely packed, highly aligned collagen fibres, indicative of mature bone structure. In contrast, newly formed bone within the defect region exhibits more disorganised collagen type I fibres with varied orientations. This pattern is observed in samples showing bone union including Delta1 + BMP-2, F35 + BMP-2, and collagen + BMP-2. Conversely, samples exhibiting non-union (Delta1, F35, and T35 + BMP-2) are characterised by a mineralised capsule with disordered collagen type I fibres and the remaining gap length filled with thin, immature collagen type III fibres. Interestingly, the presence of the T35 fragment in the hydrogel had a negative impact on the healing of the CBDs, with fewer cases of unionisation reported in T35 with low dose BMP-2 compared to its Delta1 and F35 counterpart.

3. Discussion

The confinement of BMP-2 and its efficient presentation at the cell-material interface are critical features for enhancing the effectiveness of biomaterials in treating CBDs [45]. This would allow for reduced BMP-2 dosages, thus mitigating associated health risks and financial burdens [46]. Previous research from our laboratory implemented fibronectin to a PEG hydrogel to proffer BMP-2 sequestration properties and demonstrated improved bone regeneration [11]. Here, we report the creation of a peptide-based hydrogel functionalised with a fragment of tenascin-c spanning from the 3rd to the 5th TNCIII domains. We demonstrate that this tenascin-c fragment can bind growth factors and instigate the synergistic effect to promote osteogenesis *in vitro*. Tenascin-c-functionalised hydrogels are mainly implemented in neural applications to guide neuronal differentiation and outgrowth [47–49]; however, few studies have addressed the application of tenascin-c in an osteogenic context [50], and, to the best of our knowledge, no study implemented the 3rd and 5th TNCIII domains for BMP-2-induced osteogenesis. On the other hand, the application of peptide hydrogels for bone engineering applications is increasingly explored due to the modular control these hydrogel systems offer [50–52].

Integration of the tenascin-c fragment into the fibre architecture was

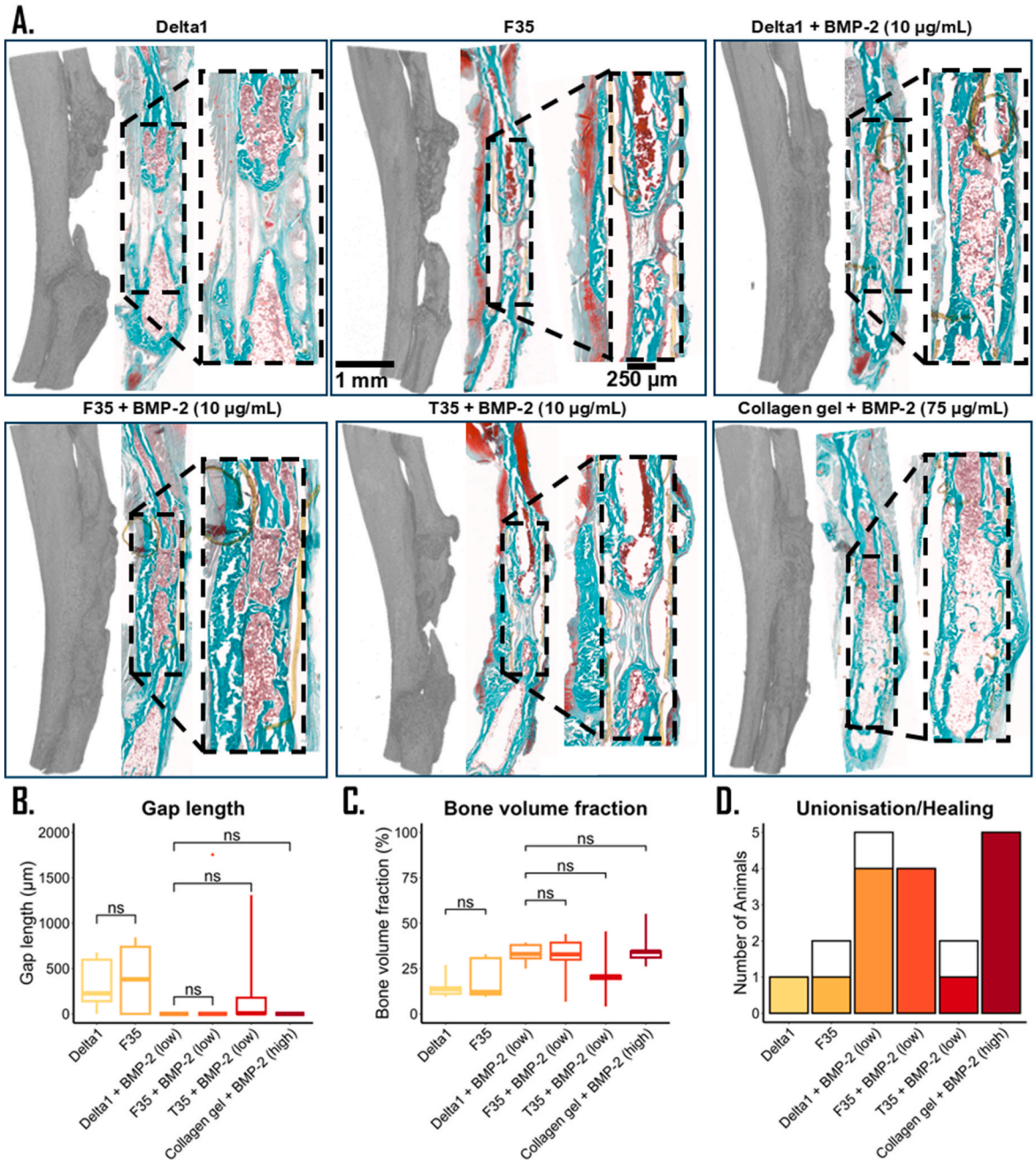

Fig. 4. Bone reconstruction in a mouse critical-sized radial bone defect model. **A.** (Left) Image of µCT dataset showing the induced bone defect for each condition. Scale bar: 1 mm. (Middle) Goldner's trichrome staining of tissue section from the same bone. Scale bar: 1 mm. (Right) Magnified image of the central 2 mm of the critical-sized defect. Frame indicates the region analysed with µCT. Scale bar: 250 µm. **B.** µCT-derived analysis of the bone regeneration within the central 2 mm of the implant tube including gap length. **C.** Bone volume to total volume within the central 2 mm of the defect. **D.** Number of animals that achieved unionisation and healing per group, bars represent the number of cases per group that achieved bridging of the gap, the filled section of the bar represents the cases that achieved a unified bone marrow cavity. n = 5 defects dataset per group. Graphs were plotted with n = 5 for each condition. Statistical significance: 'ns' $p > 0.05$.

achieved by self-functionalisation, an established approach in SAPHs that facilitates the incorporation of one or multiple molecules of interest to supramolecular peptide structures [17,18]. The tenascin-c fragments could be conveniently produced at scale using a prokaryotic expression system and retained their integrin and growth factor binding functionalities at the respective 3rd and 5th TNCIII domains as previously reported [7,53]. Self-functionalisation was achieved by addition of the fragment stock to the Delta1 hydrogel solution without further chemical reactions. The incorporation of the fragment into the fibre architecture was evaluated through a series of assays including fragment retention, TEM, FTIR, and rheology, revealing that self-functionalisation occurs without prohibiting peptide assembly and fibre construction. Interestingly, adding the F35 fragment, which is homologous to the T35 fragment, significantly increases hydrogel stiffness when compared to the T35 hydrogel. A similar interpretation is made from the loss tangent measurement, where the tanδ of Delta1 and T35 hydrogels showed no significant difference, while the F35 hydrogel was significantly more elastic. These differences suggest that F35 acts on the fibres differently than T35, advocating for self-functionalisation taking place.

The physical mixing of the T35 fragment in the hydrogel did not lead to an extensive leakage as expected, but instead, a retention of ≈85 % of the fragment content after a week of incubation with MSCs. We

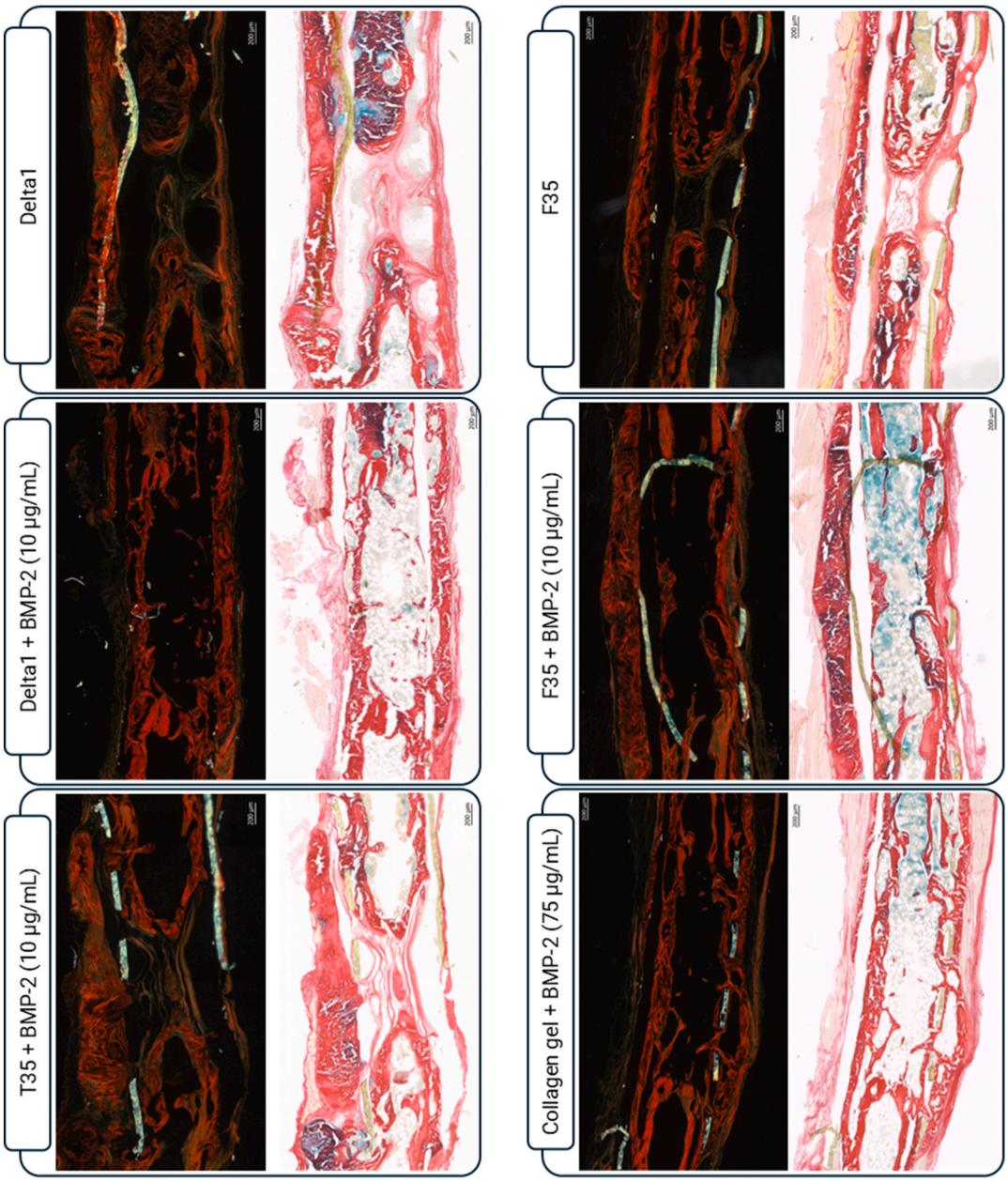

Fig. 5. Collagen architecture in the critical-sized bone defects. Histological images stained with Picrosirius Red and Alcian Blue for each hydrogel groups. Brightfield images are shown on the right, while images captured under polarised light are shown on the left. Polarised light images for birefringent collagen fibres (10× magnification) were acquired using two polariser-analyser angle combinations: 0°–45° and 45°–90°, and are presented as the sum of the two. Scale bar: 200 µm. (For interpretation of the references to colour in this figure legend, the reader is referred to the Web version of this article.)

speculate that this stems from the high-density mesh of the Delta1 SAPH system (between 10 and 20 nm), entrapping the 56 kDa protein [21]. This high-retention feature is further evidenced in the release of BMP-2 (26 kDa), where the plain Delta1 hydrogel shows ≈20 % of BMP-2 release after 24 h; this result is aligned with the literature, with reports of an 18 % release of TGF-β1 (24 kDa) from a RADA16 SAPH system at 20 mg/mL after 24 h [54], and a 25 % release of BMP-2 from a RADA16 SAPH at 15 mg/mL after 72 h [51]. Thus, Delta1, and other tightly-meshed SAPH systems, have an intrinsic propensity for macromolecule retention that will benefit BMP-2-induced bone regeneration. Aside from promoting the osteoinduction of progenitor cells *in vivo*, the high-retention feature will elicit the chemotactic effect of BMP-2 to promote cell migration to the defect site [55]. Furthermore, incorporating F35 is anticipated to lengthen the half-life of BMP-2 for a prolonged local stimulation [56]. As shown, the Delta1 hydrogel can retain 60 % of its BMP-2 content over 120 h; by comparison, the F35 hydrogel retained 92 % of its BMP-2 content over the same timeframe. The retention rates observed are a substantial improvement over previously reported hydrogel systems for growth factor retention [11,57].

We subsequently investigated the osteogenic differentiation of MSCs encapsulated in the various hydrogels over 21 days of *in vitro* incubation under BMP-2 treatment. The F35 hydrogel generated a representative mature osteoblastic phenotype that was not observed in the other hydrogel groups, indicating that the synergistic effect is mainly responsible for the phenotype observed. It was also highlighted that the bare Delta1 hydrogel lacks the bioactivity required to generate functional phenotypes, as encapsulated cells remain round and sedentary throughout the 21 days of induction, as seen in analogous literature [58]. The subsequent genotype analysis of cell populations in the various hydrogels showed similar rates of upregulation of osteogenic

genes, indicating that the encapsulated MSCs are differentiating regardless of hydrogel functionalisation. The osteogenic commitment persisting throughout the hydrogel groups is thought to result from the high BMP-2 retention ability of the Delta1 hydrogel, which can keep the growth factors confined long enough to have an impact. However, the transcriptome of a cell does not systematically extrapolate to its proteome and molecular output; this is exemplified by the scarcity of calcium deposition in the Delta1 condition with BMP-2, whereas F35 yielded prominent calcification trails in agreement with the phenotype observed. All in all, the experiment attests for the efficacy of F35 as a biomaterial platform to induce and support osteogenesis *in vitro*.

As a final experiment, the *in vivo* results report that the Delta1 hydrogel platform is proficient at regenerating murine radial CBDs, revealing an innate capacity for bone repair and a relatively high baseline of regeneration compared to other systems [11,40,41]. The *in vitro* kinetics of BMP-2 release from the hydrogel cannot be extrapolated to an *in vivo* environment, however the substantial retention of BMP-2 at the defect site is corroborated by the extent of regeneration observed between Delta1 and Delta1 + BMP-2 (10 μg/mL). The supplementation of low dose BMP-2 (10 μg/mL) to the Delta1 and F35 hydrogels produces regeneration rates analogous to the collagen gel with a high dose (75 μg/mL) of BMP-2. The functionalisation of Delta1 with the F35 fragment did not proffer a significant improvement over the bare Delta1 hydrogel, as the innate regeneration potential of Delta1 is markedly high. Intriguingly, the functionalisation of the T35 fragment became detrimental to bone regeneration and further experiments should investigate this phenomenon. Overall, the experiments demonstrated that the Delta1 SAPH system is a promising biomaterial platform for bone wound healing and should be seriously considered for further investigation in the treatment of CBDs. Future iterations of the *in vivo* work should emphasise monitoring the symptoms of BMP-2 spillage in comparison to marketed technologies.

4. Conclusion

In this study, we functionalised a peptide hydrogel with a fragment of tenascin-c to endow cell adhesion and efficient growth factor presentation for the osteogenic stimulation of MSCs and the reconstruction of CBDs. We have shown that the tenascin-c functionalisation improves the bioactivity of the hydrogels and their efficiency at conveying the BMP-2 stimulus to the embedded MSCs. Furthermore, we corroborate that the synergistic effect is key to obtaining a functional and representative osteoblastic phenotype. Finally, we demonstrate the regenerative potential of the Delta1 system to heal CBDs with low doses of BMP-2 analogously to established collagen gels with high doses of the growth factor. Conclusively, this study showcases the proficiency of the Delta1 hydrogel platform and the F35 fragment for bone engineering applications, and encourages further investigation.

5. Methodology

5.1. Plasmid construction

The encoding nucleotide sequence of the tenascin-c monomer was collected from the NCBI public database (GeneID: 3371) and trimmed down to the 3rd to 5th units of the TNCIII domains, from G2725 to C3534 (transcript variant 1; NM_002160.4); the sequence was cross-referenced against the Uniprot database (P24821) and previously published literature [59,60]. The F3, F5, and F35 fragments had the peptide sequence 5′-GGGGFEFKFEFK-3′ added at the C-terminal to make them competent for self-functionalisation; a tetraglycine spacer was installed in-between the tenascin and peptide block units for flexibility. The inserts were capped with restriction sites at the 5' (*Bam*HI) and 3' (*Xho*I) end and submitted to the Genscript Gene Synthesis service for cloning into a pGEX-6P-1 vector harbouring a GST tag. The plasmids were controlled with a sequencing certificate to validate the incorporation of the insert. A full plasmid map and amino acid sequence of the tenascin-c fragment library can be found in the Supporting Information Figure S7 and Table S1.

5.2. Fragment production

Rosetta 2 pLysS/BL21-DE3 *E. Coli* were thawed on ice for 1 h, and the plasmid was added half-way through; the cells were heat-shocked for 1 min at 42 °C followed by 5 min on ice. Transformed cells were allowed to recover for 1 h in SOC media before being inoculated in 500 mL of auto-induction LB broth (Formedium) with 100 μg/mL ampicillin. Cells were allowed to expand overnight at 37 °C under 120 rpm of orbital rotation. The cells were spun down, lysed, and sonicated; the samples were spun down to pellet the cellular debris, and the cleared supernatant was transferred to the purification facility. The purification was handled by an ÄKTA start chromatograph system (General Electric) fitted with a 1 mL sepharose column (GStrap FF, Cytiva). The eluate concentrations were quantified with a Nanodrop spectrophotometer and identified by a Coomassie-stained SDS-PAGE (Bio-Rad). Finally, the eluates were dialysed for 45 min against PBS at pH 11.5 using a Slide-A-Lyser column (Thermo Fischer Scientific). The dialysed stock of purified fragments was transferred to a low-protein-binding centrifuge tube and concentrated by liquid evaporation using a Concentrator *plus* (Eppendorf) until a protein concentration between 9 and 10 mg/mL was reached.

5.3. BMP-2 binding check

A solid-phase sandwich BMP-2 ELISA (R&D Systems) was prepared by overnight incubation of 100 μL of 2 μM fragment solution in a high-binding 96 well plate (Costar); each condition was produced in triplicate with a blank (BSA) condition serving as negative control and the provided capture antibody as positive control. The ELISA was carried out according to the manufacturer's instructions; a sample solution of 1 nM BMP-2 in PBS (R&D Systems) was added to each well. The TMB substrate incubation was terminated with a sulphuric acid solution. The absorbance at 450 nm (A450) was measured using a microplate reader (Multiskan FC, Thermo Fischer Scientific).

5.4. Hydrogel preparation

The Delta1 peptide hydrogel was kindly provided by the Polymers & Peptides research group from the University of Manchester and Cell Guidance Systems Ltd. It was received as a ready-to-use peptide solution concentrated at 20 mg/mL. 0.5 μL of 5 M NaOH per 100 μL hydrogel was added to decrease fibre stability and facilitate the subsequent fragment incorporation. Hydrogel functionalisation consisted in adding the concentrated fragment stock to the Delta1 peptide solution, followed by rigorous vortexing. The fragment concentration in the hydrogels was kept consistent with the molarity of the F35 hydrogel group, functionalised at 1 mg/mL; accordingly, the F3, F5, and T35 hydrogel group were prepared at 0.66, 0.66, and 0.98 mg/mL, respectively. The dilution factor was kept consistent across all hydrogel groups by supplementation of PBS at pH 11.5 where appropriate. A video demonstrating the extrusion of the hydrogel from a positive displacement pipette can be found in Supporting Information File S1.

5.5. Rheology

Rheological characterisation of hydrogels was performed using an Anton Paar Modular compact rheometer 302e. All measurements were carried out using an 8 mm measuring plate (Anton Parr). Prior to measurement, hydrogel disks were compressed until a sensor force of 0.1 N was measured. Then, viscoelastic properties of each hydrogel were determined using amplitude sweep tests at variable shear strain from 0.01 % to 1 % with a constant angular frequency of 10 rad/s. All measurements were performed at 37 °C and hydrogels were immersed in PBS

to prevent dehydration.

5.6. Fragment retention

The Delta1, F35, and T35 hydrogels groups were prepared as previously described, then loaded into a non-tissue-culture-treated 24 well plate in 50 μl volumes; the hydrogels were submerged in 800 μL PBS and incubated at 37 °C with 5 % CO_2. At time points 1, 24, 72, 120, and 168 h, the PBS was collected and stored, and fresh PBS was replenished for the next time point. A GST-tag solid-phase ELISA (GenScript) was conducted as per manufacturer's instructions to monitor the fragment exodus over time. The concentration-known F35 protein stock was used to produce a standard curve; the A450 sample values were correlated with the standard curve and quantified to compute the cumulative percentage of fragment released.

5.7. Cell housekeeping

Bone marrow-derived human mesenchymal stem cells (MSC) were harvested from a donor femoral head and supplied at passage 0 (P0) by PromoCell. The MSCs were expanded and sustained in basal media (DMEM) with 4.5 g/L glucose (Gibco), 11 mg/mL sodium pyruvate (Gibco), 1 % MEM non-essential amino acids (Gibco), 10 % fetal bovine serum (FBS) (Cytiva), 1 % penicillin/streptomycin (76 Units/mL and 76 μg/mL respectively) (Gibco), 2.3 mM L-glutamine (Sigma), and 0.25 μg/mL Amphotericin B (Gibco)). Basal media was replenished every 72 h, and cells were passaged at 80 % confluency. MSCs were used between passages 2 and 5, and only up to passage 3 for differentiation experiments.

5.8. Cell seeding

MSCs were passaged and automatically counted (Countess 3, Invitrogen); the cells were centrifuged and resuspended in 100 μl to achieve a high cell density and reduce the dilution factor in the hydrogel. In the previously prepared hydrogel groups, cells were consistently seeded at 1.000.000 cells/mL and rigorously vortexed; 50 μl of the cell/hydrogel mixture was formed in a non-tissue culture treated 48 well plate. The loaded gels were promptly submerged with 500 μL of appropriate media and left to incubate for 1 h in cell culture conditions, after which the media was replenished; the media was again replenished after 24 h and from there every 72 h.

5.9. MSC viability

MSCs were seeded as previously described, and the assay was replicated thrice for Day 1, 3, and 7. On the respective day, a live and dead staining solution (2 μM calcein AM and 4 μM ethidium homodimer-1 in PBS) was applied for 20 min at 37 °C. The samples were rinsed twice and imaged with an LSM 980 confocal microscope (Zeiss). Image acquisition consisted of three representative snapshots at the gel mantle and core per technical replicate; image analysis was conducted with FIJI. The viability according to the gel locus was projected from the ratio of live cells to total cells.

5.10. 3D integrin binding

MSCs were seeded as previously described and cultured for 7 days. Samples were fixed with 4 % formaldehyde for 30 min, permeabilised with 0.05 % TritonX100 (Thermo Fisher Scientific) for 15 min and blocked in 1 % BSA (R&D Systems) for 1 h. A staining solution containing 1:500 DAPI (Thermo Fisher Scientific) and 1:400 phalloidin (Invitrogen) in blocking buffer was applied for 1 h, and the samples were imaged in z-stacks of ≈51 μm with 4.07 μm interspace on an LSM 980 confocal microscope (Zeiss). Image analysis consisted in measuring cell roundness using FIJI. Cells with overlapping phalloidin signals were not considered.

5.11. Transmission electron microscopy

The hydrogel samples were diluted 100-fold with HPLC-grade water and mixed by vortex. A carbon-coated copper grid (400 mesh grid, Electron Microscopy Sciences) was subjected to a 30-s air treatment with a charge-coating process in the Glow Discharge equipment Emitech K100X. Subsequently, the grid was placed on the sample droplet for 30 s, moved to water droplets three times for washing, and subsequently transferred to a 1 % uranyl acetate droplet for 30 s. Excess liquid on the grid was blotted out with a 70 mm filter paper (Whatman), and the grid was dried prior to TEM imaging. Images were acquired using an Thermo Fisher Scientific Talos L120C with a Ceta camera system complemented with a Velox Acquisition software.

5.12. Fourier transform infrared spectroscopy

The secondary structure of plain and functionalised fibres was characterised by Attenuated Total Reflectance Fourier Transform Infrared Spectroscopy via an Alpha-P FT-IR Spectrometer (Bruker). The gel sample was pipetted to cover the crystal surface of the spectrometer, and absorbance spectra were acquired from 1400 to 1800 cm^{-1}. For each sample, 256 scans were performed with a resolution of 4 cm^{-1}, and HPLC grade water was used to record a background spectrum prior to sample analysis.

5.13. Growth factor retention

Hydrogel groups were loaded with 5 μg/ml recombinant human BMP-2 with carrier (R&D Systems) and formed in 20 μl volumes in a 96 well plate, implying a 100 ng BMP-2 content per gel. Samples were submerged in 100 μL PBS and incubated at 37 °C, and the PBS was collected after 24 h. From thereon, the PBS was collected and replenished at time points 1, 24, 48, 72, and 96 h. A solid-phase ELISA (R&D Systems) was performed as per manufacturer's instructions to monitor BMP-2 release over time.

5.14. Osteogenic differentiation of MSCs in vitro

Hydrogel groups were prepared as previously described and supplemented with recombiant human BMP-2 to a 5 μg/mL concentration. The hydrogels were seeded, loaded in 50 μl volumes, and maintained over three weeks as previously described. Conditions were replicated thrice for the time points day 7, 14, and 21.

5.15. Staining

Samples were fixed, permeabilised, blocked, and stained with DAPI and phalloidin as previously described. Samples were imaged in z-stacks of ≈183 μm with 4.22 μm interspace on an LSM 980 confocal microscope (Zeiss), and image analysis was conducted with FIJI.

5.16. Alizarin red staining

Samples were fixed as previously described and dehydrated by overnight incubation in 30 % sucrose. The samples were placed in a plastic base mould (Leica Biosystems), embedded in OCT compound (Tissue-Tek), and snap-frozen in liquid nitrogen. Samples were cryosectioned on a Expredia™ CryoStar™ NX70 cryostat in 20 μm sections. Sections were subsequently left to dry for 2 h, washed in PBS for 10 min, and contoured with hydrophobic ink (A-PAP Pen; Cosmo Bio). Alizarin red staining solution was prepared by dissolving 1.44 g of Alizarin red powder (Merck) in 100 mL MilliQ, adjusting the pH to 4.2, and filtering the solution through a filter paper. The staining solution was applied to the sections for 5 min, followed by 5 rinses in MilliQ and subsequently

imaged on an EVOS XL Core.

5.17. Reverse transcription and quantitative PCR

The hydrogels were digested in pronase (5 mg/mL) (Merck) for 10 min at 37 °C, the RNA was subsequently extracted using the TriZol method. Recovered RNA was reverse translated to a cDNA library using the QuantiTect Reverse Transcription Kit (Qiagen), as per manufacturer's instructions. Samples were then used in the qPCR assay to quantify the expression of RPL13A (housekeeping gene), ALP, OPN, OSX, and OCN; primer sequences can be found in Supporting Information Table S2. The ΔCt values were calculated from the difference in Ct of the gene of interest and the housekeeping gene. The ΔΔCt was calculated by subtracting the ΔCt of the control Delta1 to the ΔCt of the treated group.

5.18. Murine critical-sized bone defect model

The experiment was conducted under the Animals (Scientific Procedures) ACT 1986 (ASPel project license n° PP5891831). All research conducted complied with ethical regulations approved by the ethical committee of the University of Glasgow.

5.19. Implant preparation

Porous polyimide tubes (for detailed dimensions, see Supporting Information Figure S6) were cut into 4 mm segments, rinsed in absolute ethanol, sonicated for 20 min, and autoclaved at 121 °C for 15 min. Peptide hydrogels were prepared as previously described for the following conditions: Delta1, F35, Delta1 + BMP-2 (10 μg/mL), F35 + BMP-2 (10 μg/mL), and T35 + BMP-2 (10 μg/mL). All conditions used recombinant human BMP-2 with carrier from R&D Systems. A collagen hydrogel + BMP-2 (75 μg/mL) serving as positive control was prepared through the following protocol: all reagents and materials were kept on ice. 1 mL of rat tail collagen type I (First Link Ltd.) was aliquoted into a 15 mL tube, to which 400 μL of 0.1 M NaOH (Honeywell) was added, followed by 200 μL of ×10 DMEM (low glucose; Sigma); the addition of the DMEM turned the solution yellow. The collagen solution was titrated with 0.1 M NaOH until it turned pink. The collagen solution was supplemented with BMP-2 to reach the desired growth factor concentration while maintaining a pH of 7.

In sterile conditions, autoclaved implant tubes were filled with 3 μL of hydrogel mixture. Implants carrying the peptide hydrogel conditions were left to incubate at 37 °C in PBS overnight; implants with the collagen hydrogel were incubated for 10 min at 37 °C next to wet paper towel to prevent drying out. Prepared implants were submerged in sterile PBS and stored at 4 °C until the next day where they were transferred to the operating theatre.

5.20. Radial defect surgery

C57BL/6 male and female mice (8 weeks old, Charles River) were anesthetized with isoflurane gas and their right forelimbs were shaved and disinfected with povidone-iodine. Mice received a subcutaneous dose of buprenorphine and carprofen for analgesia prior to surgery. A skin incision was made along the forearm, and soft tissue was carefully separated using a periosteal elevator to expose the radius. A 2.5 mm defect was created at the midpoint of the radius using a custom-made parallel double-bladed bone cutter, ensuring the ulna remained intact. The 4 mm-long implant tube was then positioned between the proximal and distal ends of the defect. The muscle and skin were repositioned, and the incision was closed with degradable sutures. Post-surgery, mice were monitored for signs of distress, mobility, and weight loss. After eight weeks, mice were euthanized, and forelimb bone samples were explanted, fixed in 4 % formaldehyde, and stored in 70 % ethanol for further analysis. Six mice (3 males and 3 females) were used per experimental condition.

5.21. Micro-computed tomography (μCT)

Defects were μCT scanned at a resolution (voxel side length) of 3 μm with the Skyscan 1172 desktop system (Bruker, Kontich, Belgium) equipped with the 80 Vp/100 μA Hamamatsu X-ray tube. All defects were scanned with the following settings: 60 kVp tube voltage, 100 μA tube current, 1750 ms exposure time, 0.3° rotation step size for 180°, with two frame averages performed per rotation. A 0.5 mm thick aluminium filter was placed before the X-ray source. Acquired projection images were reconstructed using Skyscan NRecon software (Version 1.6.9.18, Bruker) into 8-bit grayscale images, with ring-artefact reduction and beam hardening correction set to 13 and 40 %, respectively. Subsequently, reconstructed datasets were co-registered to ensure that all datasets were spatially aligned. Specifically, a representative dataset was selected and used as the reference standard dataset. This dataset was manually aligned such that its z-axis corresponded with the long axis of the radius bone in DataViewer software (Version 1.5.6.2, Bruker). All other datasets were rigidly co-registered against this reference dataset in a semi-automated fashion in DataViewer.

Newly formed bone was quantified within the central 2 mm of the polyimide tube, using a cylindrical volume of interest (VOI) with height 2 mm and diameter 0.9 mm in CTAnalyser software (Version 1.18.8.0, Bruker). The outline of the polyimide tube is observable in the μCT dataset, hence the VOI follows this outline. Morphometric analysis was then performed on this VOI after binarisation via a global threshold (min set to 85 and max set to 255), and two despeckle operations: removal of white and black speckles (in 3D) less than 50 voxels in size, respectively. Outcome measures include the ratio of bone volume to tube volume (BV/TV), TV being the cylindrical VOI, and gap length, which excluded any unconnected bone. Tissue mineral density (TMD) was determined following the μCT scanning of two 2 mm diameter calibration hydroxyapatite rods (Bruker) with known densities of 0.25 and 0.75 g cm^{-3}, respectively, with the same scanner settings described above. One defect from each group contained an abscess, which was omitted from the analysis. All groups thus had five defects analysed (n = 5).

5.22. Histology

Non-demineralised bone specimens were processed for cold polymethyl methacrylate (PMMA) embedding following manufacturer instructions (Technovit 9100, Morphisto GmbH, Germany). Briefly, samples were dehydrated in an ascending ethanol series, stained with rhodamine solution [0.417 g of Rhodamine B (Fisher Scientific SL, Spain) per 100 mL of ethanol], cleared with xylene, and embedded in polymerised PMMA [61].

Consecutive and numbered PMMA embedded longitudinal sections (6 μm in thickness) were cut in the microtome (Model RM2255, Leica Biosystems, Spain) and dried at 60 °C for 48 h. Serial histological sections were stained with Goldner's Trichrome and Alcian blue + Picrosirius Red stainings. Stained slides were imaged with an Axio Observer 7 microscope (Zeiss, Spain) at ×10 magnification both with bright field and using polarised light microscopy for Alcian Blue and Picrosirius staining.

Goldner's Trichrome stain was used to visualise tissue structure and morphology. The following tissue types could be stained: collagen (green), osteoid (red), cell nuclei (black), and cell cytosol (bright red). Alcian blue + Picrosirius Red staining was used to visualise the distribution and the type of collagen. In the bright field, cell nuclei (black), collagen (red), and proteoglycan-rich cartilage matrix (blue) could be observed. With polarised light, thick and mature collagen fibres (orange-reddish) and thinner and more immature fibres (green) were visualised [44]. Polarised light images were taken two polariser-analyser combinations, 0-45° and 45-90° respectively, and merging both images afterwaerds for representation.

5.23. Statistical analysis

Unless stated otherwise, all *in vitro* experiments were conducted in technical triplicates. Obtained datasets were first tested for normality with a Shapiro-Wilk test and homogeneity of variance with a Levene's test. Comparison of three or more groups with normal distribution and equal variances was performed with a one-way ANOVA test and corrected with a Tukey's test. If the dataset followed Gaussian distribution but with heterogeneous variances, a Welch's ANOVA test corrected with Tukey's test was performed instead. The comparison of three or more groups with non-normal distribution was performed with a Kruskal-Wallis' test corrected with a Dunn's test; the same test would be performed in case of unequal variances. Statistical differences among groups were denoted by 'ns', *, **, ***, and **** indicating a respective p-value of >0.05, <0.05, 0.01, 0.001, and 0.0001.

CRediT authorship contribution statement

Alexandre Trubert-Paneli: Writing – original draft, Methodology, Investigation, Formal analysis, Data curation, Conceptualization. **Jonathan A. Williams:** Methodology, Investigation. **James F.C. Windmill:** Resources. **Leire Iturriaga:** Methodology, Investigation. **Eonan W. Pringle:** Methodology, Investigation. **Theodora Rogkoti:** Writing – review & editing, Methodology. **Siyuan Dong:** Methodology, Investigation. **Amaia Cipitria:** Writing – review & editing, Methodology, Investigation. **Aline F. Miller:** Methodology, Investigation. **Cristina Gonzalez-Garcia:** Writing – review & editing, Methodology, Investigation, Data curation. **Alberto Saiani:** Writing – review & editing, Supervision, Investigation. **Manuel Salmeron-Sanchez:** Writing – review & editing, Supervision, Methodology, Investigation, Conceptualization.

Declaration of competing interest

The authors declare the following financial interests/personal relationships which may be considered as potential competing interests: Manuel Salmeron-Sanchez reports financial support was provided by European Research Council. Manuel Salmeron-Sanchez reports financial support was provided by Engineering and Physical Sciences Research Council. Manuel Salmeron-Sanchez is on the international editoral board of Biomaterials. If there are other authors, they declare that they have no known competing financial interests or personal relationships that could have appeared to influence the work reported in this paper.

Acknowledgements

The work was supported by funding from the European Union's Horizon 2020 research and innovation programme (Grant agreement No. 874889 - HEALIKICK), European Research Council AdG (101054728) and EPSRC through the Transformative Healthcare Technologies Programme Grant 'Mechanomeds' (EP/X033554/1). C.G-G. acknowledges support from the Engineering and Physical Sciences Research Council (Grant No. EPSRC NIA – EP/T000457/1). A.T.P. acknowledges the companies Manchester BIOGEL Ltd. and Cell Guidance Systems Ltd. for their support. IBEC is member of CERCA Programme/Generalitat de Catalunya.

Appendix A. Supplementary data

Supplementary data to this article can be found online at https://doi.org/10.1016/j.biomaterials.2025.123553.

Data availability

Data will be made available on request.

References

[1] P. Baldwin, D.J. Li, D.A. Auston, H.S. Mir, R.S. Yoon, K.J. Koval, Autograft, allograft, and bone graft substitutes: clinical evidence and indications for use in the setting of orthopaedic trauma surgery, J. Orthop. Trauma 33 (2019) 203–213, https://doi.org/10.1097/BOT.0000000000001420.
[2] C. Mauffrey, B.T. Barlow, W. Smith, Management of segmental bone defects, J. Am. Acad. Orthop. Surg. 23 (2015) 143–153, https://doi.org/10.5435/JAAOS-D-14-00018R1.
[3] W.F. McKay, S.M. Peckham, J.M. Badura, A comprehensive clinical review of recombinant human bone morphogenetic protein-2 (INFUSE® Bone Graft), Int. Orthop. 31 (2007) 729–734, https://doi.org/10.1007/s00264-007-0418-6.
[4] N. Epstein, Complications due to the use of BMP/INFUSE in spine surgery: the evidence continues to mount, Surg. Neurol. Int. 4 (2013) 343, https://doi.org/10.4103/2152-7806.114813.
[5] M.M. Martino, J.A. Hubbell, The 12th–14th type III repeats of fibronectin function as a highly promiscuous growth factor-binding domain, FASEB J. 24 (2010) 4711–4721, https://doi.org/10.1096/fj.09-151282.
[6] J. Ishihara, A. Ishihara, K. Fukunaga, K. Sasaki, M.J.V. White, P.S. Briquez, et al., Laminin heparin-binding peptides bind to several growth factors and enhance diabetic wound healing, Nat. Commun. 9 (2018) 2163, https://doi.org/10.1038/s41467-018-04525-w.
[7] L. De Laporte, J.J. Rice, F. Tortelli, J.A. Hubbell, Tenascin C promiscuously binds growth factors via its fifth fibronectin type III-like domain, PLoS One 8 (2013) e62076, https://doi.org/10.1371/journal.pone.0062076.
[8] P.M. Comoglio, C. Boccaccio, L. Trusolino, Interactions between growth factor receptors and adhesion molecules: breaking the rules, Curr. Opin. Cell Biol. 15 (2003) 565–571, https://doi.org/10.1016/S0955-0674(03)00096-6.
[9] M.M. Martino, F. Tortelli, M. Mochizuki, S. Traub, D. Ben-David, G.A. Kuhn, et al., Engineering the growth factor microenvironment with fibronectin domains to promote wound and bone tissue healing, Sci. Transl. Med. 3 (2011), https://doi.org/10.1126/scitranslmed.3002614.
[10] V. Llopis-Hernández, M. Cantini, C. González-García, Z.A. Cheng, J. Yang, P. M. Tsimbouri, et al., Material-driven fibronectin assembly for high-efficiency presentation of growth factors, Sci. Adv. 2 (2016) e1600188, https://doi.org/10.1126/sciadv.1600188.
[11] S. Trujillo, C. Gonzalez-Garcia, P. Rico, A. Reid, J. Windmill, M.J. Dalby, et al., Engineered 3D hydrogels with full-length fibronectin that sequester and present growth factors, Biomaterials 252 (2020) 120104, https://doi.org/10.1016/j.biomaterials.2020.120104.
[12] K.S. Midwood, M. Chiquet, R.P. Tucker, G. Orend, Tenascin-C at a glance, J. Cell Sci. 129 (2016) 4321–4327, https://doi.org/10.1242/jcs.190546.
[13] F.S. Jones, P.L. Jones, The tenascin family of ECM glycoproteins: structure, function, and regulation during embryonic development and tissue remodeling, Dev. Dyn. 218 (2000) 235–259, https://doi.org/10.1002/(SICI)1097-0177(200006)218:2<235::AID-DVDY2>3.0.CO;2-G.
[14] P. Weber, D.R. Zimmermann, K.H. Winterhalter, L. Vaughan, Tenascin-C binds heparin by its fibronectin type III domain five, J. Biol. Chem. 270 (1995) 4619–4623, https://doi.org/10.1074/jbc.270.9.4619.
[15] A. Aggeli, I.A. Nyrkova, M. Bell, R. Harding, L. Carrick, T.C.B. McLeish, et al., Hierarchical self-assembly of chiral rod-like molecules as a model for peptide β-sheet tapes, ribbons, fibrils, and fibers, Proc. Natl. Acad. Sci. 98 (2001) 11857–11862, https://doi.org/10.1073/pnas.191250198.
[16] X. Zhao, S. Zhang, L. Spirio, PuraMatrix: self-assembling peptide nanofiber scaffolds, in: P. Ma, J. Elisseeff (Eds.), Scaffolding Tissue Eng, CRC Press, 2005, pp. 217–238, https://doi.org/10.1201/9781420027563.ch15.
[17] C. Hickling, H.S. Toogood, A. Saiani, N.S. Scrutton, A.F. Miller, Nanofibrillar peptide hydrogels for the immobilization of biocatalysts for chemical transformations, Macromol. Rapid Commun. 35 (2014) 868–874, https://doi.org/10.1002/marc.201400027.
[18] G.A. Hudalla, T. Sun, J.Z. Gasiorowski, H. Han, Y.F. Tian, A.S. Chong, et al., Gradated assembly of multiple proteins into supramolecular nanomaterials, Nat. Mater. 13 (2014) 829–836, https://doi.org/10.1038/nmat3998.
[19] C.M. Rubert Pérez, Z. Álvarez, F. Chen, T. Aytun, S.I. Stupp, Mimicking the bioactivity of fibroblast growth Factor-2 using supramolecular nanoribbons, ACS Biomater. Sci. Eng. 3 (2017) 2166–2175, https://doi.org/10.1021/acsbiomaterials.7b00347.
[20] R. Liu, G.A. Hudalla, Using self-assembling peptides to integrate biomolecules into functional supramolecular biomaterials, Molecules 24 (2019) 1450, https://doi.org/10.3390/molecules24081450.
[21] J. Gao, C. Tang, M.A. Elsawy, A.M. Smith, A.F. Miller, A. Saiani, Controlling self-assembling peptide hydrogel properties through network topology, Biomacromolecules 18 (2017) 826–834, https://doi.org/10.1021/acs.biomac.6b01693.
[22] J.K. Wychowaniec, A.M. Smith, C. Ligorio, O.O. Mykhaylyk, A.F. Miller, A. Saiani, Role of sheet-edge interactions in β-sheet self-assembling peptide hydrogels, Biomacromolecules 21 (2020) 2285–2297, https://doi.org/10.1021/acs.biomac.0c00229.
[23] A. Maslovskis, J.-B. Guilbaud, I. Grillo, N. Hodson, A.F. Miller, A. Saiani, Self-assembling peptide/thermoresponsive polymer composite hydrogels: effect of peptide–polymer interactions on hydrogel properties, Langmuir 30 (2014) 10471–10480, https://doi.org/10.1021/la502358b.
[24] A. Barth, Infrared spectroscopy of proteins, Biochim. Biophys. Acta BBA Bioenergy 1767 (2007) 1073–1101, https://doi.org/10.1016/j.bbabio.2007.06.004.

[25] A. Saiani, A. Mohammed, H. Frielinghaus, R. Collins, N. Hodson, C.M. Kielty, et al., Self-assembly and gelation properties of α-helix versus β-sheet forming peptides, Soft Matter 5 (2009) 193–202, https://doi.org/10.1039/B811288F.
[26] S. Dong, S.L. Chapman, A. Pluen, S.M. Richardson, A.F. Miller, A. Saiani, Effect of peptide–polymer host–guest electrostatic interactions on self-assembling peptide hydrogels structural and mechanical properties and polymer diffusivity, Biomacromolecules 25 (2024) 3628–3641, https://doi.org/10.1021/acs.biomac.4c00232.
[27] A.Y. Clark, K.E. Martin, J.R. García, C.T. Johnson, H.S. Theriault, W.M. Han, et al., Integrin-specific hydrogels modulate transplanted human bone marrow-derived mesenchymal stem cell survival, engraftment, and reparative activities, Nat. Commun. 11 (2020) 114, https://doi.org/10.1038/s41467-019-14000-9.
[28] T.P. Kunzler, T. Drobek, M. Schuler, N.D. Spencer, Systematic study of osteoblast and fibroblast response to roughness by means of surface-morphology gradients, Biomaterials 28 (2007) 2175–2182, https://doi.org/10.1016/j.biomaterials.2007.01.019.
[29] O. Dobre, M.A.G. Oliva, G. Ciccone, S. Trujillo, A. Rodrigo-Navarro, D.C. Venters, et al., A hydrogel platform that incorporates laminin isoforms for efficient presentation of growth factors – neural growth and osteogenesis, Adv. Funct. Mater. 31 (2021) 2010225, https://doi.org/10.1002/adfm.202010225.
[30] B. Kulterer, G. Friedl, A. Jandrositz, F. Sanchez-Cabo, A. Prokesch, C. Paar, et al., Gene expression profiling of human mesenchymal stem cells derived from bone marrow during expansion and osteoblast differentiation, BMC Genom. 8 (2007) 70, https://doi.org/10.1186/1471-2164-8-70.
[31] M. Valenti, L. Dalle Carbonare, M. Mottes, Osteogenic differentiation in healthy and pathological conditions, Int. J. Mol. Sci. 18 (2016) 41, https://doi.org/10.3390/ijms18010041.
[32] W. Liu, L. Zhang, K. Xuan, C. Hu, L. Li, Y. Zhang, et al., Alkaline phosphatase controls lineage switching of mesenchymal stem cells by regulating the LRP6/GSK3β complex in hypophosphatasia, Theranostics 8 (2018) 5575–5592, https://doi.org/10.7150/thno.27372.
[33] Q. Liu, M. Li, S. Wang, Z. Xiao, Y. Xiong, G. Wang, Recent advances of osterix transcription factor in osteoblast differentiation and bone formation, Front. Cell Dev. Biol. 8 (2020) 601224, https://doi.org/10.3389/fcell.2020.601224.
[34] C. Zhang, Transcriptional regulation of bone formation by the osteoblast-specific transcription factor Osx, J. Orthop. Surg. 5 (2010) 37, https://doi.org/10.1186/1749-799X-5-37.
[35] M. Fakhry, Molecular mechanisms of mesenchymal stem cell differentiation towards osteoblasts, World J. Stem Cell. 5 (2013) 136, https://doi.org/10.4252/wjsc.v5.i4.136.
[36] W. Orapiriyakul, M.P. Tsimbouri, P. Childs, P. Campsie, J. Wells, M.A. Fernandez-Yague, et al., Nanovibrational stimulation of mesenchymal stem cells induces therapeutic reactive oxygen species and inflammation for three-dimensional bone tissue engineering, ACS Nano 14 (2020) 10027–10044, https://doi.org/10.1021/acsnano.0c03130.
[37] J.P. Stains, R. Civitelli, Cell-cell interactions in regulating osteogenesis and osteoblast function, Birth Defects Res. Part C Embryo Today - Rev. 75 (2005) 72–80, https://doi.org/10.1002/bdrc.20034.
[38] D. Kudelska-Mazur, M. Lewandowska-Szumieł, M. Mazur, J. Komender, Osteogenic cell contact with biomaterials influences phenotype expression, Cell Tissue Bank. 6 (2005) 55–64, https://doi.org/10.1007/s10561-005-1911-z.
[39] Y. Yang, X. Wang, Y. Wang, X. Hu, N. Kawazoe, Y. Yang, et al., Influence of cell spreading area on the osteogenic commitment and phenotype maintenance of mesenchymal stem cells, Sci. Rep. 9 (2019) 6891, https://doi.org/10.1038/s41598-019-43362-9.
[40] S.O. Sarrigiannidis, O. Dobre, A.R. Navarro, M.J. Dalby, C. Gonzalez-Garcia, M. Salmeron-Sanchez, Engineered dual affinity protein fragments to bind collagen and capture growth factors, Mater. Today Bio 20 (2023) 100641, https://doi.org/10.1016/j.mtbio.2023.100641.
[41] U. Dhawan, J.A. Williams, J.F.C. Windmill, P. Childs, C. Gonzalez-Garcia, M. J. Dalby, et al., Engineered surfaces that promote capture of latent proteins to facilitate integrin-mediated mechanical activation of growth factors, Adv. Mater. 36 (2024) 2310789, https://doi.org/10.1002/adma.202310789.
[42] A. Shekaran, J.R. García, A.Y. Clark, T.E. Kavanaugh, A.S. Lin, R.E. Guldberg, et al., Bone regeneration using an alpha 2 beta 1 integrin-specific hydrogel as a BMP-2 delivery vehicle, Biomaterials 35 (2014) 5453–5461, https://doi.org/10.1016/j.biomaterials.2014.03.055.
[43] J.R. García, A.Y. Clark, A.J. García, Integrin-specific hydrogels functionalized with VEGF for vascularization and bone regeneration of critical-size bone defects, J. Biomed. Mater. Res. 104 (2016) 889–900, https://doi.org/10.1002/jbm.a.35626.
[44] L.C.U. Junqueira, G. Bignolas, R.R. Brentani, Picrosirius staining plus polarization microscopy, a specific method for collagen detection in tissue sections, Histochem. J. 11 (1979) 447–455, https://doi.org/10.1007/BF01002772.
[45] A.W. James, G. LaChaud, J. Shen, G. Asatrian, V. Nguyen, X. Zhang, et al., A review of the clinical side effects of bone morphogenetic Protein-2, Tissue Eng., Part B 22 (2016) 284–297, https://doi.org/10.1089/ten.teb.2015.0357.
[46] K.S. Cahill, Prevalence, complications, and hospital charges associated with use of bone-morphogenetic proteins in spinal fusion procedures, JAMA 302 (2009) 58, https://doi.org/10.1001/jama.2009.956.
[47] E.J. Berns, Z. Álvarez, J.E. Goldberger, J. Boekhoven, J.A. Kessler, H.G. Kuhn, et al., A tenascin-C mimetic peptide amphiphile nanofiber gel promotes neurite outgrowth and cell migration of neurosphere-derived cells, Acta Biomater. 37 (2016) 50–58, https://doi.org/10.1016/j.actbio.2016.04.010.
[48] M. Sever, G. Gunay, M.O. Guler, A.B. Tekinay, Tenascin-C derived signaling induces neuronal differentiation in a three-dimensional peptide nanofiber gel, Biomater. Sci. 6 (2018) 1859–1868, https://doi.org/10.1039/C7BM00850C.
[49] K. Glotzbach, A. Faissner, Substrate-bound and soluble domains of tenascin-C regulate differentiation, proliferation and migration of neural stem and progenitor cells, Front. Cell. Neurosci. 18 (2024) 1357499, https://doi.org/10.3389/fncel.2024.1357499.
[50] M. Sever, B. Mammadov, M.O. Guler, A.B. Tekinay, Tenascin-C mimetic peptide nanofibers direct stem cell differentiation to osteogenic lineage, Biomacromolecules 15 (2014) 4480–4487, https://doi.org/10.1021/bm501271x.
[51] M.C. Phipps, F. Monte, M. Mehta, H.K.W. Kim, Intraosseous delivery of bone morphogenic Protein-2 using a self-assembling peptide hydrogel, Biomacromolecules 17 (2016) 2329–2336, https://doi.org/10.1021/acs.biomac.6b00101.
[52] M. Halperin-Sternfeld, A. Pokhojaev, M. Ghosh, D. Rachmiel, R. Kannan, I. Grinberg, et al., Immunomodulatory fibrous hyaluronic acid- Fmoc -diphenylalanine-based hydrogel induces bone regeneration, J. Clin. Periodontol. 50 (2023) 200–219, https://doi.org/10.1111/jcpe.13725.
[53] P. Joshi, C.-Y. Chung, I. Aukhil, H.P. Erickson, Endothelial cells adhere to the rgd domain and the fibrinogen-like terminal knob of tenascin, J. Cell Sci. 106 (1993) 389–400, https://doi.org/10.1242/jcs.106.1.389.
[54] A. Zhou, S. Chen, B. He, W. Zhao, X. Chen, D. Jiang, Controlled release of TGF-beta 1 from RADA self-assembling peptide hydrogel scaffolds, Drug Des. Dev. Ther. 10 (2016) 3043–3051, https://doi.org/10.2147/DDDT.S109545.
[55] J. Fiedler, G. Röderer, K. Günther, R.E. Brenner, BMP-2, BMP-4, and PDGF-bb stimulate chemotactic migration of primary human mesenchymal progenitor cells, J. Cell. Biochem. 87 (2002) 305–312, https://doi.org/10.1002/jcb.10309.
[56] G.S. Schultz, A. Wysocki, Interactions between extracellular matrix and growth factors in wound healing, Wound Repair Regen. 17 (2009) 153–162, https://doi.org/10.1111/j.1524-475x.2009.00466.x.
[57] M.M. Martino, P.S. Briquez, A. Ranga, M.P. Lutolf, J.A. Hubbell, Heparin-binding domain of fibrin(ogen) binds growth factors and promotes tissue repair when incorporated within a synthetic matrix, Proc. Natl. Acad. Sci. 110 (2013) 4563–4568, https://doi.org/10.1073/pnas.1221602110.
[58] L.A. Castillo Diaz, M. Elsawy, A. Saiani, J.E. Gough, A.F. Miller, Osteogenic differentiation of human mesenchymal stem cells promotes mineralization within a biodegradable peptide hydrogel, J. Tissue Eng. 7 (2016) 2041731416649789, https://doi.org/10.1177/2041731416649789.
[59] D.E. Nies, T.J. Hemesath, J.H. Kim, J.R. Gulcher, K. Stefansson, The complete cDNA sequence of human hexabrachion (Tenascin). A multidomain protein containing unique epidermal growth factor repeats, J. Biol. Chem. 266 (1991) 2818–2823, https://doi.org/10.1016/S0021-9258(18)49920-6.
[60] J.R. Gulcher, D.E. Nies, M.J. Alexakos, N.A. Ravikant, M.E. Sturgill, L.S. Marton, et al., Structure of the human hexabrachion (tenascin) gene, Proc. Natl. Acad. Sci. 88 (1991) 9438–9442, https://doi.org/10.1073/pnas.88.21.9438.
[61] I. Moreno-Jiménez, D.S. Garske, C.A. Lahr, D.W. Hutmacher, A. Cipitria, Targeted 2D histology and ultrastructural bone analysis based on 3D microCT anatomical locations, MethodsX 8 (2021) 101480, https://doi.org/10.1016/j.mex.2021.101480.